https://doi.org/10.22226/2410-3535-2023-1-39-44

Physico-chemical properties of silicon-carbon films obtained by electrochemical deposition

I. Yu. Bogush[†,1], N. K. Plugotarenko[1], T. N. Myasoedova[1], V. V. Ptashnik[2]

[†]inlys@sfedu.ru

[1]Institute of Nanotechnologies, Microelectronics and Equipment Engineering, Southern Federal University, Taganrog, 347900, Russia

[2]Joint Stock Company, Taganrog Scientific-Research Institute of Communication, Taganrog, 347913, Russia

Pure silicon-carbon films and the films doped with manganese or nickel were deposited on a copper foil by the electrochemical method from a methanol/hexamethyldisilazane solution. Scanning electron microscopy studies of silicon-carbon films showed a complex structure due to the presence of three-dimensional agglomerates and "leafy" structures. Raman spectroscopy showed that the silicon-carbon films were highly defective. The porosity study revealed that all samples mostly contained mesopores with sizes of 10 – 50 nm. The nickel-containing samples showed a more stable bimodal distribution of the mesopores. The highest specific surface area was observed for the manganese-containing silicon carbon films.

Keywords: silicon-carbon film, supercapacitor electrode material, mesoporous material.

1. Introduction

Alternative energy sources such as supercapacitors are promising for the future because of their high storage capacity, power density and low cost of fabrication [1]. However, the low energy density of supercapacitors limits their practical application [2]. In addition, the properties of an active material used to produce the electrodes are very important for the fabrication of supercapacitors. Therefore, many researchers are concentrating on improving the properties of electrode materials for supercapacitors [3 – 5].

Carbon materials such as carbon fiber, graphene, and carbon microspheres have such advantages as high chemical stability and good electrical conductivity. This makes such materials a good choice for electrode materials in supercapacitors [6 – 9]. Consequently, diamond-containing silicon-carbon films attract much attention as promising materials due to their unique properties: hardness (≈20 – 40 GPa) chemical stability, band gap width, low friction coefficient and thermal stability (at least 300°C) [10].

Electrodes based on silicon-carbon films can provide higher capacitance due to fast and reversible redox reaction [11]. Similarly, silicon-carbon films can be modified with metal atoms to improve the properties of the electrodes. Among a wide range of transition metals manganese and nickel are the most promising pseudo-capacitance materials having a high specific capacity, low cost, environmental safety, and availability in large quantities in nature [12 – 16]. Carbon materials can be synthesized with a wide range of morphologies. So, the relationships between the morphology, phase content, type of metal atom and electrochemical characteristics of the electrode material are to be investigated [17].

There are several methods for silicon-carbon film production, such as ion-beam sputtering, magnetron sputtering, pulsed laser deposition, and chemical vapor deposition [18]. However, the use of these methods is limited due to the need of complex equipment and harsh experimental conditions, including a high vacuum and high temperature. Materials which are deposited from the vapor phase can also be deposited in the liquid phase by using galvanic techniques and vice versa [19]. From the application viewpoint, the liquid deposition techniques have many advantages over the vapor deposition techniques such as a possibility of a large area deposition on intricate surfaces, low deposition temperature, low consumption of energy, and the simplicity of the setup [18]. Thus, electrochemical deposition methods based on the use of organic electrolytes deserve special attention. The electrosynthesis of any material depends on the electrolyte, electrode material, temperature, the nature of the precursor, additives and basic electrochemical parameters [20]. Electrochemical methods make it possible to carry out synthesis in one stage. Thus, it is possible to produce silicon-carbon films of different compositions by varying the experimental conditions.

The presence of silicon and carbon in the precursor composition is very important for the electrochemical deposition of silicon-carbon films. Precursors that are used for the chemical vapor deposition can also be used for the electrochemical deposition of silicon-carbon films. Hexamethyldisilazane, tetramethyldisilazane, hexamethylcyclotrisilazane [21, 22], tetraethyl orthosilicate [23] are used as sources of silicon atoms. Such organic substances as methanol, ethanol are used as solvents and carbon sources [20]. Nickel foam, copper foil, silicon, etc. act as substrates for electrochemical deposition.

It is known that thin films containing micro-, meso- and macro-pores have improved characteristics for energy distribution and storage [20]. The morphology investigation of silicon-carbon films requires obtaining a good characterization of the distribution of pores. One of the most popular and relatively simple methods for evaluating the porous structure is based on the analysis of the adsorption isotherms of nitrogen. Unfortunately, obtaining and verifying the pore size distribution on silicon-carbon films is a difficult task, since the molecular arrangements that occur are highly disordered and very complex and indirect techniques that are used in the study of the porosity are also complex [18]. Therefore, extracting structure-property relationships for these materials is an interesting challenge due to the complex structure of the silicon-carbon films.

In the previous works a number of properties were investigated and the possibility of using silicon-carbon films obtained by electrochemical deposition as supercapacitor electrodes was shown [24, 25].

The present work is devoted to a study on the relationship between the structure and porosity of silicon-carbon materials obtained by electrochemical deposition and their electrochemical characteristics as supercapacitor electrodes.

2. Materials and experimental methods

2.1. Fabrication of the silicon-carbon films

The process of electrochemical deposition of silicon-carbon films was described earlier in the works [24 – 26]. A copper foil as the substrate was mounted on the negative electrode, and a plate of pyrolytic graphite was mounted on the positive electrode. The metal-containing films were deposited in two stages. At the first stage, the silicon-carbon film from the methanol/hexamethyldisilane (HMDS) solution in the ratio of 9:1 or 2:1 was deposited for about 30 minutes at 180 V. At the second stage, $Ni(NO_3)_2 \cdot 6H_2O$ (0.01%) or $MnSO_4 \cdot 5H_2O$ (0.05%) were added to the solution and then deposited for 5 –10 minutes at 40 and 60 V, respectively. The choice of voltage depends on the composition and conductivity of the electrolytes. When metal salt is added, the conductivity increases, and therefore the voltage required to initiate the deposition process decreases. The supercapacitor electrode samples were fabricated with the size of $28 \times 12 \times 0.5$ mm^3.

2.2. Material characterization

The surface morphology was studied using a scanning electron microscope Nova NanoLab 600 (FEI Company, Netherlands). The structure characteristics were measured by Raman spectroscopy using a Raman microscope, 2 cm^{-1} resolution, 514 nm laser (Renishaw plc, UK). The pore size distribution and specific surface area were determined using Quantachrome Nova 2000E Surface Area (Quantachrome Instruments, USA) by adsorption/desorption isotherms using the Barrett-Joyner-Halenda (BJH) method, uncertainty of measurement was ±5%. In comparison, the pore size distribution was calculated using DFT (density functional theory). A three electrode cell consisting of a commercial Ag/AgCl (3 M KCl) electrode as the reference electrode, and a carbon electrode as the counter electrode were used. Cyclic voltammetry (CV) and galvanostatic charge-discharge tests were performed using an Ellins P-45X potentiostat/galvanostat (Electrochemical Instruments, Russia) at room temperature in 8M NaOH solution within a potential window of 0.5 V, scan rate from 20 to 100 mV/s and current density from 430 to 860 mA/g.

3. Results and discussion

From the structural formula of methanol, it follows that under the influence of high voltages the -CH_3 groups are detached. CH_3 groups concentrate at the cathode-solution interface, partially dissociating into atomic components and gradually passing to the cathode surface. Also, under high voltage, the HMDS molecule dissociates into functional groups Si-C and Si-N, which pass to the cathode surface forming silicon-containing clusters $(SiC)_x$ and $(SiN)_x$ on it. So, these electrochemical reactions contribute to the growth of the film on the surface of the substrate mounted on the cathode.

The results of the surface morphology investigations are shown in Fig. 1. SEM investigation showed a developed surface morphology characterized by three-dimensional agglomerates and irregular-shaped pores. The samples based on the pure silicon-carbon films deposited from a solution with a methanol : HMDS ratio of 2:1 (Fig. 1a) have a "leafy" structure. The samples with the methanol : HMDS ratio of 9:1 (Fig. 1b) reveal the grain morphology. The morphology of the films containing manganese (Fig. 1c) is presented by three-dimensional agglomerates and needle-like nanolayers. Ni-containing films (Fig. 1d) are characterized by a multi-level porous structure with the grains inside the pores. The thickness of the films estimated by the interferometer technique was shown to be 350 and 800 nm for pure, manganese- and nickel-doped silicon-carbon films, respectively. The electrochemical characteristics of carbon materials are significantly affected by their porous structure.

The pore size distribution and pore volume obtained by the BJH method for silicon carbon films are shown in Fig. 2 a. All samples showed a distribution of pores in the range of 10 – 50 nm with a maximum at about 13 nm. The existence of the mesopores can contribute to charge storage, which leads to a significant acceleration of electrolyte ion transport [27, 28]. The volume of micropores is approximately 4 – 5% of the total pores volume. The macropores were observed in all the samples except the sample obtained from methanol/HMDS 9:1 and not exceeds 3% of the total volume. Silicon-carbon films doped with nickel were characterized by a bimodal distribution of the pores in the area of mesopores with maximums at 13 and 22 nm, as well as by the largest volume of mesopores, $1.43 \cdot 10^{-4}$ mm^3/g. The smallest mesopore volume was observed in the manganese-containing film ($8.76 \cdot 10^{-5}$ mm^3/g) characterized by the highest specific surface area of 165 m^2/g^{-3} due to the macropores contribution. The largest micropore volume of $1.4 \cdot 10^{-4}$ mm^3/g and the highest specific surface area of mesopores (83 m^2/g^{-3}) were observed for the silicon-carbon films obtained from the solution with a methanol : HMDS ratio of 2:1.

The investigation of Raman spectra showed that the silicon-carbon films were heterogeneous objects. The Raman

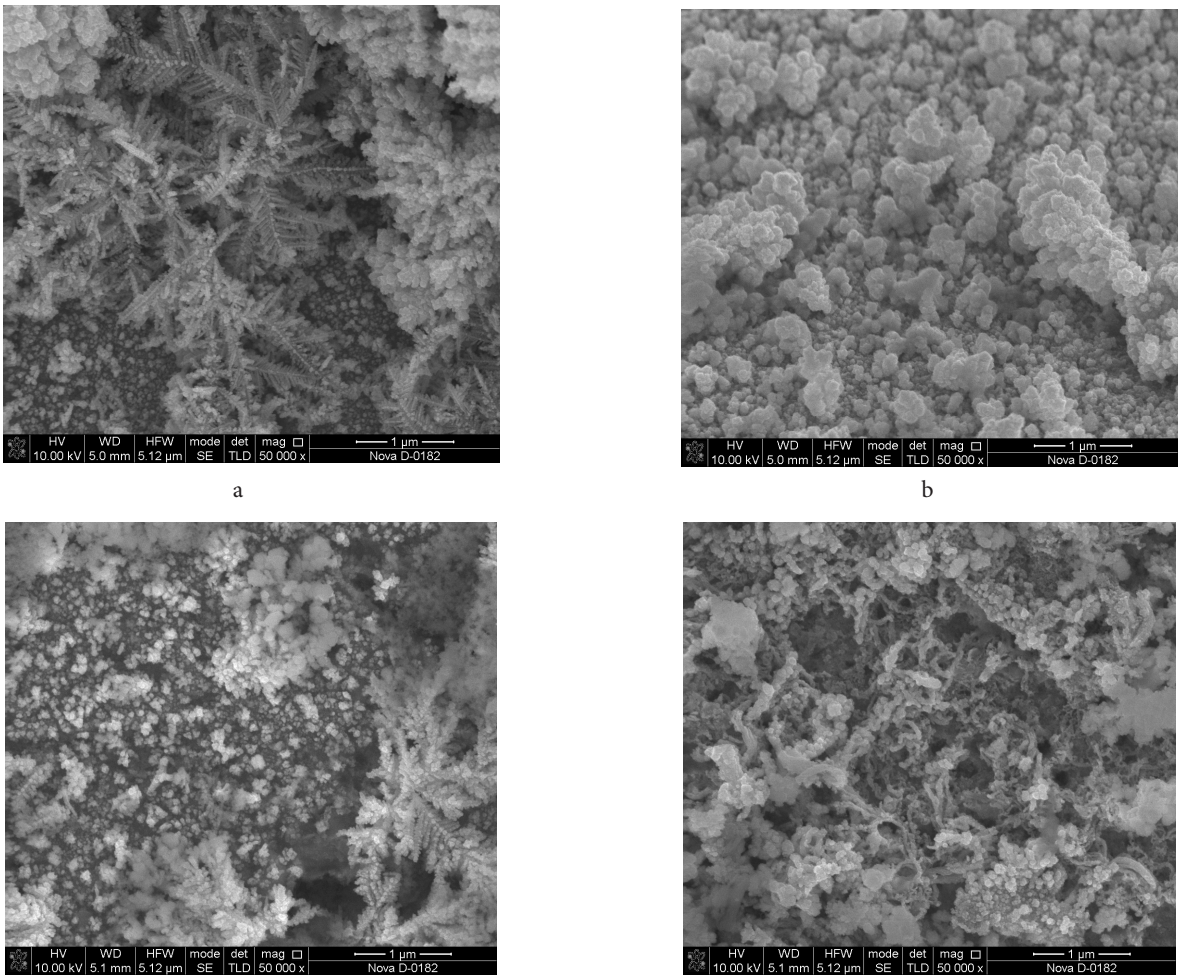

Fig. 1. SEM images of silicon-carbon films from the methanol/hexamethyldisilane (HMDS) solution in the ratio of 2:1 (a); 9:1 (b) at 180 V and from the methanol/hexamethyldisilane (HMDS) solution in the ratio of 9:1 with additional manganese at 60 V (c); nickel at 40 V (d).

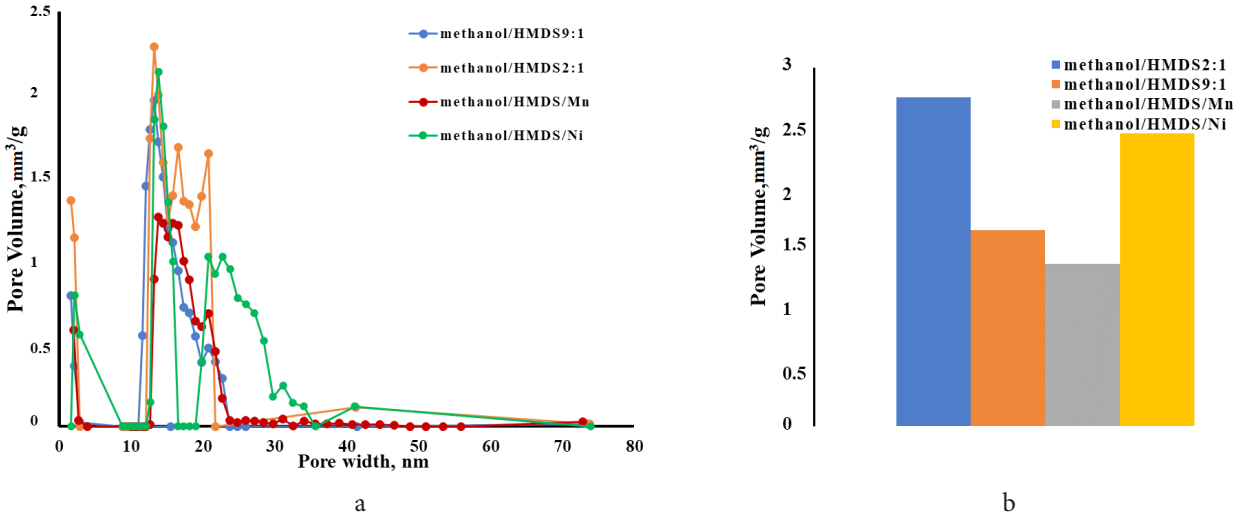

Fig. 2. (Color online) Pore size distribution of silicon-carbon films (a), pore volume of silicon-carbon films (b).

spectra (Fig. 3) contain lines characteristic for SiC polytypes. The samples were characterized by the presence of the hexagonal 6H SiC polytype with a 15R SiC rhombohedral phase impurities. Deconvolution was carried out on the minimum number of Gaussian peak components for which their resulting curve described the experimental curve with a confidence of >99%. Therefore, three peaks at 1361, 1524, and 1627 cm^{-1} were observed. The peaks around 1361 and 1524 cm^{-1} correspond to the D and G bands. The broadening of the G band on the higher wave number side is explained by the presence of the D' band at 1627 cm^{-1}. The appearance of the D' peak proves that silicon-carbon films are highly defective structures [29]. The films deposited from the solution with the methanol/HMDS ratio of 2:1 are amorphous and the

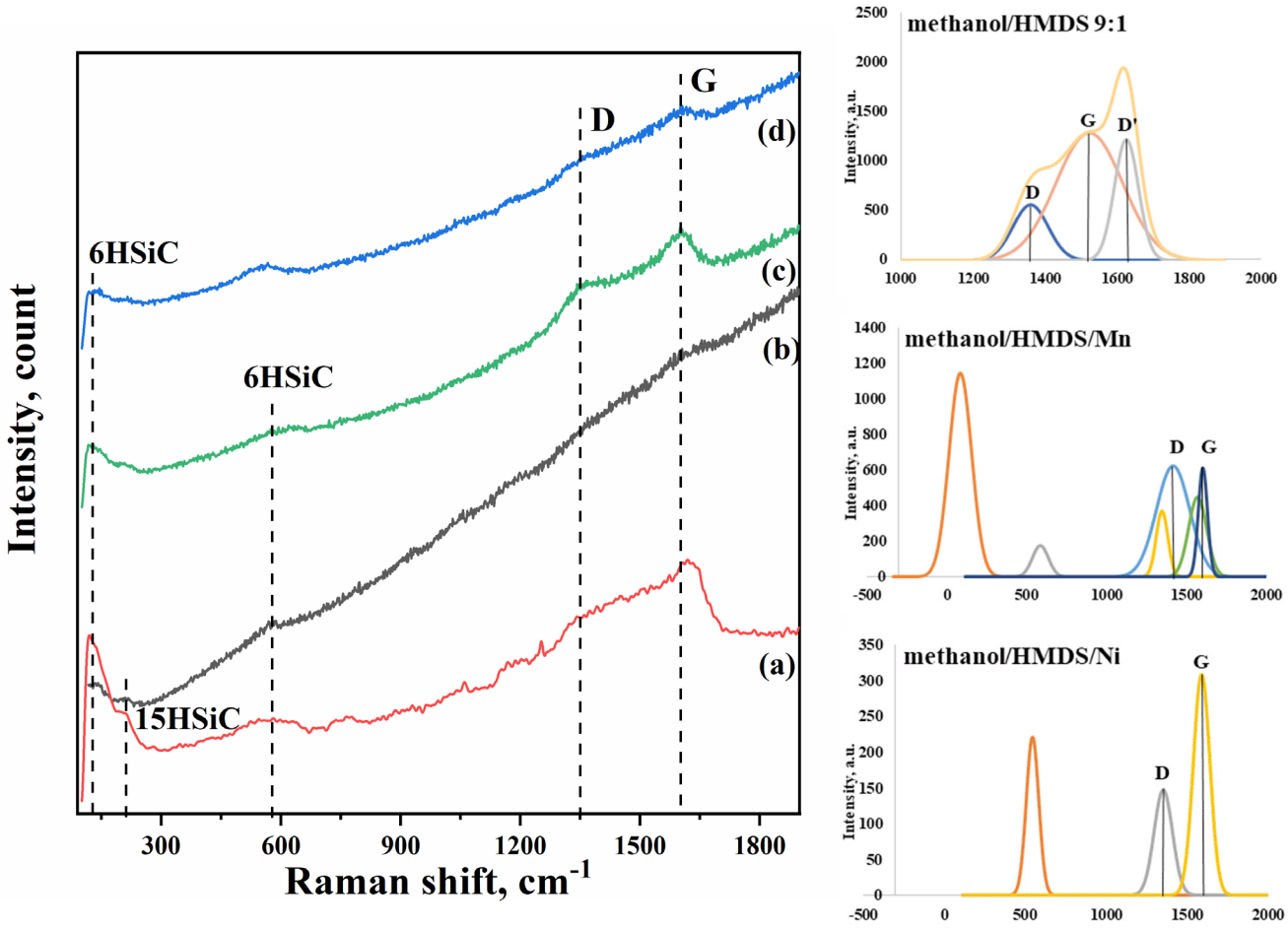

Fig. 3. (Color online) Raman spectra with the deconvolution of the D and G peaks (under the Raman spectra) for silicon-carbon films from the methanol/hexamethyldisilane (HMDS) solution in the ratio of 9:1 (a); 2:1 (b) and from the methanol/hexamethyldisilane (HMDS) solution in the ratio of 9:1 with additional manganese (c); nickel (d).

carbon phase is not present. Thus, peaks responsible for the hexagonal phase of the 6H SiC polytype are observed at 151, 218 and 573 cm^{-1} (Fig. 3 a).

Two characteristic carbon peaks at ≈1360 and ≈1580 cm^{-1} wave numbers were detected in the manganese- and nickel-doped samples, which are defined as D and G peaks, respectively. The D peak arises from out-of-plane oscillations due to the presence of structural disorder (structural defects, edge effects, and sp^2 hanging carbon bonds). The G peak arises from out-of-plane oscillations of sp^2 carbon atoms, which are often found in graphite materials [30]. A higher level of disorder in the graphite plane leads to a broadening of G and D bands with a higher relative intensity [31]. The Raman spectrum of the nickel-containing sample contains D and G peaks in the 1377 and 1609 cm^{-1} area, respectively. In the manganese-containing sample, the broad D and G bands can be deconvoluted into four components: D2, D1, G2, and G1 with centers at 1308, 1433, 1581, and 1613 cm^{-1}, respectively. D2 and G2 bands indicate that the films contain a certain number of defects [29]. I_D/I_G ratio calculated from the Raman spectra was to be ≈1 and 0.45 for manganese and nickel doped samples, respectively. The smaller ratio corresponds to smaller free carbon clusters [32], and also reveals a structure with smaller number of defects. The peaks corresponding to the hexagonal phase of the 4H SiC polytype were observed in both metal-containing samples in the 560 – 590 cm^{-1} region [33].

The cyclic voltammetry (CVA) and galvanostatic charge/discharge curves are presented in Fig. 4. As can be seen from Fig. 4 a, the CVA curves of silicon-carbon films show pseudocapacitive behavior. The magnitude of the redox peaks was greatest for the nickel-containing sample corresponding to the reversible Faradic redox reaction $NiO + OH^- \leftrightarrow NiOOH + e^-$ [34]. The charge/discharge curves (Fig. 4 b) confirm the greater contribution of the manifestation of pseudocapacitance properties for this sample. The specific capacitance of the electrode calculated by the CV curves was to be 427, 362, 490, 525 F/cm^2 for the methanol/HMDS 2:1, methanol/HMDS 9:1, methanol/HMDS/Ni and methanol/HMDS/Mn samples, respectively. The ratio between the discharge and charge capacities is ≈70%. The charge/discharge curves (Fig. 4 b) of the electrodes based on the pure silicon carbon films have more linear character. The discharge of the electrical double layer is the primary process in these samples [35].

The samples demonstrated a high stability. As a result, after 450 charge-discharge cycles, the capacity of test samples decreased by 3% and 2% for methanol/HMDS/Mn and methanol/HMDS/Ni samples, respectively.

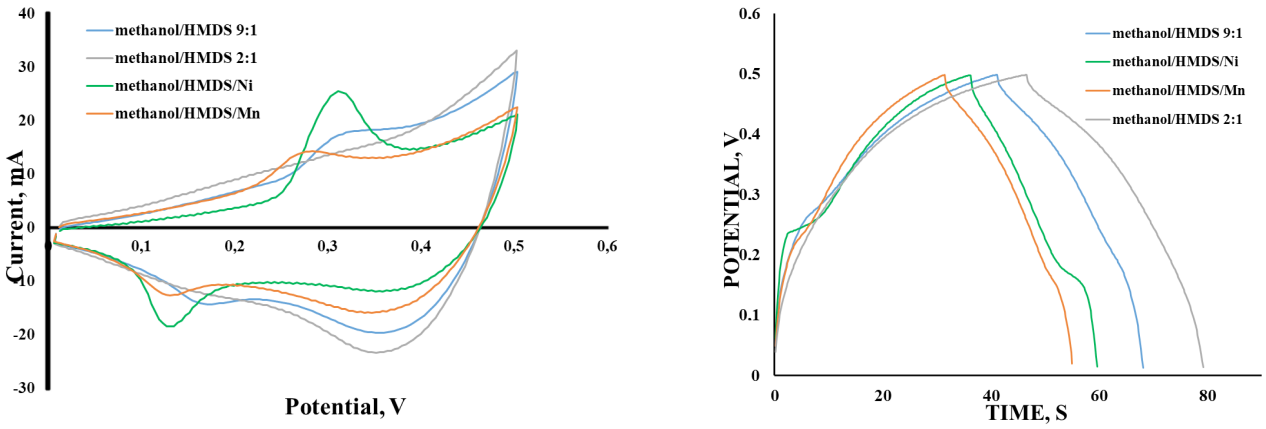

a b

Fig. 4. (Color online) CVA curves of supercapacitor electrodes (80 mV/s) (a); charge/discharge curves of supercapacitors electrodes (430 mA/g) (b).

4. Conclusions

Pure silicon-carbon films and the films doped with manganese or nickel were deposited on the copper foil by electrochemical method from methanol/hexamethyldisilazane solution. The films reveal mesoporous structure characterized by high defectiveness. Presence of hexagonal 6H SiC polytype with a 15R SiC rhombohedral phase impurities was observed by Raman spectrometry. Investigations by cyclic voltammetry and galvanostatic charge-discharge methods showed that silicon-carbon films have pseudocapacitive properties and can be used as materials for supercapacitor electrodes.

It was found that high specific surface area of meso- and micropores was observed for the electrode methanol/HMDS 2:1. The loading of metals to the films increased the capacitance of the electrodes. The specific surface area of the manganese-containing silicon-carbon film was higher than that of the other samples. Investigations of the stability of silicon-carbon materials showed the promise of nickel-containing samples. It is less defective and has a more stable bimodal size distribution of mesopores.

In conclusion, we successfully investigated silicon-carbon films and proved their performance as material for supercapacitor. In the future, we will continue the stability investigation, as well as the development test samples of supercapacitors based on silicon-carbon film and the study of their characteristics.

Acknowledgements. The research was supported by the Strategic Academic Leadership Program of the Southern Federal University ("Priority 2030").

References

1. T. Lin, I. W. Chen, F. Liu, C. Yang, H. Bi, F. Xu, F. Huang. Science. 350, 1508 (2015). Crossref
2. V. Subramanian, C. Luo, A. M. Stephan, K. Nahm, S. Thomas, B. Wei. J. Phys. Chem. C. 111, 7527 (2007). Crossref
3. M. Yu, Y. Han, Y. Li, J. Li, L. Wang. Carbohyd. Polym. 199, 555 (2018). Crossref
4. L. L. Zhang, X. Zhao. Chem. Soc. Rev. 38, 2520 (2009). Crossref
5. T. Kim, G. Jung, S. Yoo, K. S. Suh, R. S. Ruoff. ACS Nano. 7, 6899 (2013). Crossref
6. Q. Cao, Y. Zhang, J. Chen, M. Zhu, C. Yang, H. Guo, Y. Song, Y. Li, J. Zhou. Ind. Crops Prod. 148, 112181 (2020). Crossref
7. X. Li, W. Zhang, M. Wu, S. Li, X. Li, Z. Li. Int. J. Biol. Macromol. 183, 950 (2021). Crossref
8. J. Xia, N. Zhang, S. Chong, Y. Chen, C. Sun. Green Chemistry. 20, 694 (2018). Crossref
9. C. C. Viggi, S. Simonetti, E. Palma, P. Pagliaccia, C. Braguglia, S. Fazi, S. Baronti, M. A. Navarra, I. Pettiti, C. Koch et al. Biotechnol. Biofuels. 10, 303 (2017). Crossref
10. A. Berrueta, A. Ursua, I. San Martin, A. Eftekhari, P. Sanchis. IEEE Access. 7, 50869 (2019). Crossref
11. C. B. Amara, H. Hammami, S. Fakhfakh, et al. J. Electron. Mater. 50, 5915 (2021). Crossref
12. C. Wu, Y. Zhu, M. Ding, C. Jia, K. Zhang. Electrochim. Acta. 291, 249 (2018). Crossref
13. Q. X. Xia, K. S. Hui, K. N. Hui, S. D. Kim, J. H. Lim, Y. C. Si, et al. J. Mater. Chem. 2, 22102 (2015). Crossref
14. G. Gao, H. B. Wu, S. Ding, L. M. Liu, X. W. Lou. Small. 11 (7), 804 (2014). Crossref
15. L. Deng, H. Qu, Y. Zhang, S. Jiao, X. Zhang, K. Liu, et al. J. Solid State Chem. 281, 121026 (2018). Crossref
16. M. Feng, J. Gu, G. C. Zhang, M. Xu, Y. Yu, X. Liu, et al. J. Solid State Chem. 282, 121084 (2020). Crossref
17. F. Naseri, S. Karimi, E. Farjah, E. Schaltz. Renew. Sust. Energ. Rev. 155, 111913 (2022). Crossref
18. X. B. Yan, B. K. Tay, G. Chen, S. R. Yang. Electrochem. Commun. 8 (5), 737 (2006). Crossref
19. H. Zhuang, N. Yang, L. Zhang, R. Fuchs, X. Jiang. Appl. Mater. Int. 7 (20), 10886 (2015). Crossref
20. C.-H. Chang, B. Hsia, J. P. Alper, S. Wang, L. E. Luna, C. Carraro, S.-Y. Lu, R. Maboudian. ACS Appl. Mater. Int. 7(48), 26658 (2015). Crossref
21. T. Nakayamada, K. Matsuo, Y. Hayashi, A. Izumi, Y. Kadotani. Thin solid films. 516, 656 (2008). Crossref
22. S. Manocha, D. Ankur, L. M. Manocha. Eurasian Chem Tech Journal. 13, 27 (2011). Crossref

23. J. J. Senkevich, et al. Applied Physics A: Mat. Sc. 77 (3), 581 (2003). Crossref
24. M. N. Grigoryev, T. N. Myasoedova, T. S. Mikhailova. J. Phys.: Conf. Ser. 1124, 081043 (2018).
25. N. K. Plugotarenko, T. N. Myasoedova, I. Y. Bogush. Materials Science in Semiconductor Processing. 135, 106121 (2021). Crossref
26. T. N. Myasoedova, M. N. Grigoryev, T. S. Mikhailova. Journal of Alloys and Compounds. 855 (2), 157504 (2021). Crossref
27. M. S. Javed, S. S. A. Shah, S. Hussain. Chemical Engineering Journal. 382,122814 (2020). Crossref
28. J. Jagiello, A. Chojnacka, S. E. M. Pourhosseini, Z. Wang, F. Beguin. Carbon. 178, 113 (2021). Crossref
29. A. Kaniyoor, S. Ramaprabhu. Aip Adv. 2, 032183 (2012). Crossref
30. V. Georgakilas, J. A. Perman, J. Tucek, R. Zboril. Broad Chemical Reviews. 115, 4744 (2015). Crossref
31. K. N. Kudin, et al. Nano Letters. 8, 36 (2008). Crossref
32. A. C. Ferrari, D. M. Basko. Nat Nano. 8, 235 (2015). Crossref
33. M. Iijima, H. Kamiya. J. Phys. Chem. C. 112, 11786 (2008). Crossref
34. M. Yu, W. Wang, C. Li, et al. Asia Mater. 6, e129 (2014). Crossref
35. S. Lafon-Placette, K. Delbé, J. Denape, M. Ferrato. Journal of the European Ceramic Society. 35 (4), 1147 (2014). Crossref